# BRACELET BUS-NA 98 BZ 23 - BRONZE - IRON AGE - SWITZERLAND

**Artefact name** Bracelet bus-na 98 BZ 23

**Authors** Christian. Degrigny (HE-Arc CR, Neuchâtel, Neuchâtel, Switzerland) & Naima. Gutknecht (HE-Arc CR, Neuchâtel, Neuchâtel, Switzerland) & Valentina. Valbi (Laboratoire Métallurgie et Culture LMC-IRAMAT-CNRS-UTBM, Belfort, Franche-Comté, France)

**Url** /artefacts/1009/

## The object




*Credit Service archéologique de l'Etat de Fribourg, M-J.Scholl.*

Fig. 1: Fragment of a deburred bracelet (side A) from Bussy/Pré de Fond (Switzerland),

## Description and visual observation

**Description of the artefact** Fragment of a deburred bracelet with irregular curvature; surface of side A with a central rib and hammer marks; surface of side B flat; triangular section.

**Type of artefact** Jewellery

**Origin** Bussy/Pré de Fond, Fribourg, Fribourg, Switzerland

**Recovering date** 1998

**Chronology category** Iron Age

**chronology tpq** 550 B.C.

**chronology taq** 450 B.C.

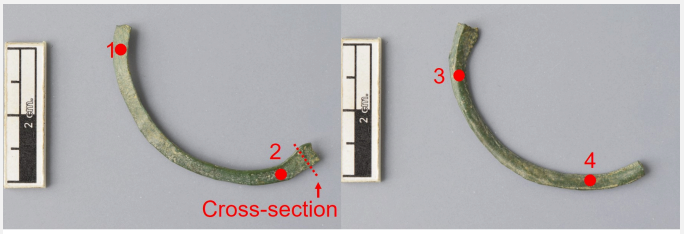

This work is licensed under CC BY-NC-ND 4.0

| | |
|---|---|
| **Chronology comment** | First Iron Age - Hallstatt Culture (Ha D2-3) |
| **Burial conditions / environment** | Soil |
| **Artefact location** | Archaeological Service of the Fribourg Canton, Fribourg |
| **Owner** | Archaeological Service of the Fribourg Canton, Fribourg |
| **Inv. number** | bus-na 98 BZ 23 |
| **Recorded conservation data** | Mechanical cleaning of the external corrosion products and soils |

**Complementary information**

None.

## Study area(s)




*Credit Service archéologique de l'Etat de Fribourg, M-J.Scholl/HE-Arc CR, N.Gutknecht.*

Fig. 2: Side B (left) and side A (right) of bracelet showing the sampling area and the XRF analysis areas (red dots),

## Binocular observation and representation of the corrosion structure

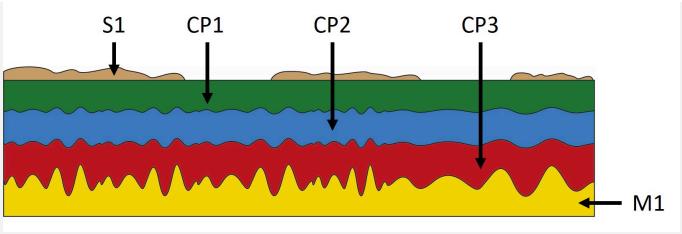
The schematic representation below gives an overview of the corrosion structure encountered on the bracelet from a first visual macroscopic observation.

| Strata | Type of stratum | Principal characteristics |
|---|---|---|
| S1 | Soil | light brown, thin, non-compact, powdery |
| CP1 | Corroded product | dark green, medium, continuous, compact, soft |
| CP2 | Corroded product | blue, thin, continuous, compact, very soft |
| CP3 | Corroded product | red, thin, continuous, compact, hard |
| M1 | Metal | dark yellow, metallic, compact, soft |

Table 1: Description of the principal characteristics of the strata as observed under binocular and described according to Bertholon's method.

The transition between CP3 and the metal M1 is irregular and rough.


This work is licensed under CC BY-NC-ND 4.0




*Credit HE-Arc CR, N.Gutknecht.*

Fig. 3: Stratigraphic representation of the corrosion structure of the bracelet by macroscopic and binocular observation,

## MiCorr stratigraphy(ies) – Bi

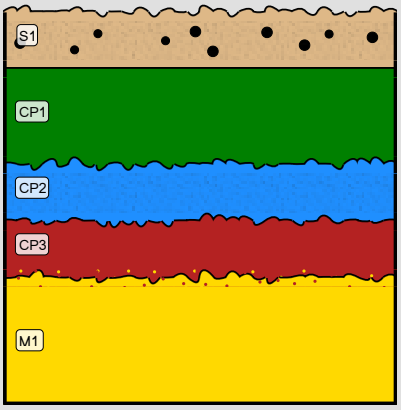
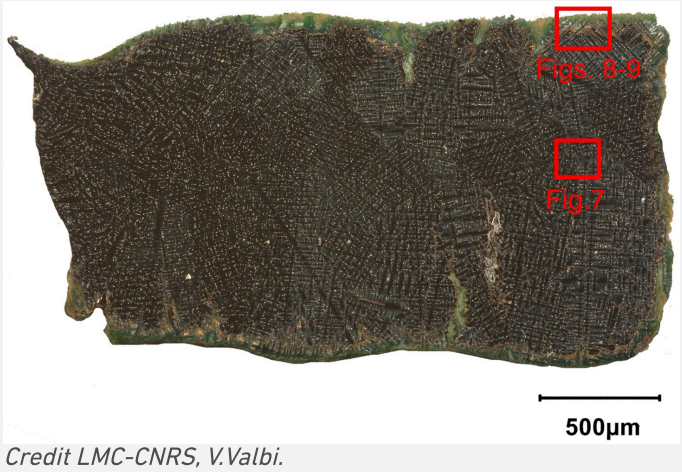



Fig. 4: Stratigraphic representation of the corrosion structure of the bracelet observed macroscopically under binocular microscope using the MiCorr application with reference to the whole Fig. 3. The characteristics of the strata are only accessible by clicking on the drawing that redirects you to the search tool by stratigraphy representation, Credit HE-Arc CR, N.Gutknecht.

## Sample(s)




*Credit LMC-CNRS, V.Valbi.*

Fig. 5: Micrograph of the cross-section of the sample taken from the bracelet (Fig. 2) in dark field showing the location of Fig. 7 to 9,

| | |
|---|---|
| **Description of sample** | The cross-section corresponds to a lateral cut (Fig. 2) and is representative of the entire thickness of the bracelet's body. A metallic core is present below the corrosion layers (Fig. 6). |
| **Alloy** | Bronze |
| **Technology** | As-cast |
| **Lab number of sample** | ébauche 23 |
| **Sample location** | Archaeological Service of the Fribourg Canton, Fribourg |


This work is licensed under CC BY-NC-ND 4.0

| | |
|---|---|
| **Responsible institution** | Archaeological Service of the Fribourg Canton, Fribourg |
| **Date and aim of sampling** | February 2020. Metallographic study. |

**Complementary information**

None.

## Analyses and results

*Analyses performed*:

**Non-invasive approach**

- XRF with handheld portable X-ray fluorescence spectrometer (NITON XL3t 950 Air GOLDD+, Thermo Fischer®). General Metal mode, acquisition time 60s (filters: Li20/Lo20/M20)

**Invasive approach (on the sample)**

- Optical microscopy: the sample is polished, then it is observed on a numerical microscope KEYENCE VHX-7000 in bright and dark field.
- Metallography: the polished sample is etched with alcoholic ferric chloride and observed by optical microscopy in bright field.
- SEM-EDS: the sample is coated with a carbon layer and analysis are performed on a SEM-FEG JEOL 7001-F equipped with a silicon-drift EDS Oxford detector (Aztec analysis software) with an accelerating voltage of 20 kV and probe current at about 9 nA. The relative error is considered of about 10% for content range <1mass%, and of 2% for content range of >1mass%.
- µ-Raman spectroscopy: it is performed on a HORIBA Labram Xplora spectrometer equipped with a 532 nm laser with 1800 grating, the laser power employed is between 0.04 and 0.55 mW with acquisition time varying between 1 and 5 minutes.

## Non invasive analysis

The XRF analysis on the bracelet was carried out before sampling on four areas (Fig. 2). All strata (soil, corrosion products, and metal) are analyzed at the same time. The metal is presumably a copper-tin alloy with some lead, while the other elements detected (Fe, Si, P, Al) are from the burial environment.

| Elements (mass %) | 1 | 2 | 3 | 4 |
|---|---|---|---|---|
| Cu | 51 | 45 | 48 | 44 |
| Sn | 25 | 27 | 28 | 26 |
| Pb | 3 | 3 | 3 | 3 |
| Fe | 2 | 3 | 2 | 3 |
| Si | 10 | 12 | 10 | 12 |
| P | 3 | 3 | 2 | 3 |
| Al | 4 | 5 | 4 | 6 |

Table 2: Chemical composition of the surface of the bracelet at four representative points shown in Fig.2. Method of analysis: XRF. The results are rounded up to the nearest whole number.

## Metal

EDX analysis (Table 3) of the residual metal on cross-section indicates that it is a high tin bronze (13 mass% Sn) with lead (1 mass% Pb).


This work is licensed under CC BY-NC-ND 4.0

The metal has a dendritic structure (Fig. 6). Different dendritic grains are observed (with boundaries visible on Fig. 7).
The α phase constitutes the dendrites, the α+δ phase (grey) is observed in interdendritic areas.

Small Pb inclusions (2-3 µm, Fig. 7) are homogeneously distributed on the whole surface of the sample.

Selective corrosion of the α phase is locally observed following the dendritic microstructure (Fig. 8).

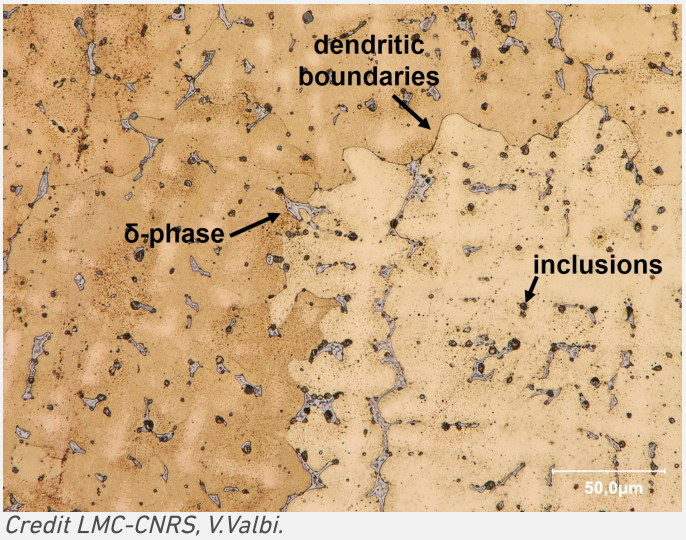
| Elements | mass % |
|---|---|
| Cu | 84 |
| Sn | 13 |
| Pb | 1.2 |
| Ni | <0.5 |
| As | <0.5 |
| Si | <0.5 |
| S | <0.5 |
| Si | <0.5 |

Table 3: Chemical composition (mas%) of the alloy over a general area of analysis obtained by SEM-EDX.




*Credit LMC-CNRS, V.Valbi.*

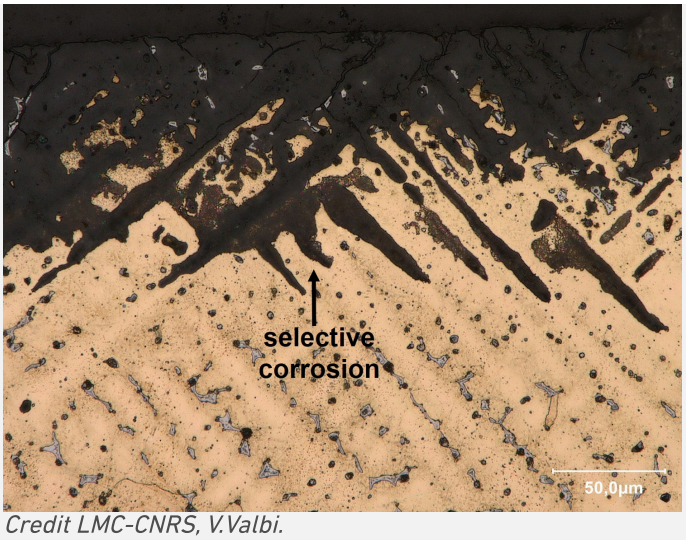
Fig. 6: Micrograph of the etched cross-section of the sample taken from the bracelet (Fig. 2) in bright field,




*Credit LMC-CNRS, V.Valbi.*

Fig. 7: Micrograph of the metal sample from Fig. 5 (detail), etched, bright field, dendritic structure. Presence of grey Sn-rich α+δ phase and black Pb inclusions,


This work is licensed under CC BY-NC-ND 4.0




*Credit LMC-CNRS, V.Valbi.*

Fig. 8: Micrograph of the metal sample from Fig. 5 (detail), etched, bright field, showing the presence of selective corrosion,

| | |
|---|---|
| **Microstructure** | Dendritic structure with inclusions |
| **First metal element** | Cu |
| **Other metal elements** | Sn, Pb |

### Complementary information

The interface roughness between the metal and the CPs, corresponding to the stratum identified as corroded metal (CM1) was measured through optical microscopy observations and the following parameters were determined (in µm): Rp=105, Rv = 19, Rt = 124, Ra = 32.

## Corrosion layers

The observation of the sample in cross-section in dark field (Figs. 5 and 9) allowed to identify an external continuous green stratum (CP1), a red discontinuous thin stratum (CP2) and a corroded metal area (CM1) with an interface following the metal dendritic structure. The EDX elemental analysis (Table 4) and mapping (Fig. 10) of the visually identified CPs show that CP1 is Cu depleted, O and Sn enriched and polluted with Si, Ca, Fe and P. No EDX analysis is available for CP2. These results are in agreement with the preliminary XRF analysis.

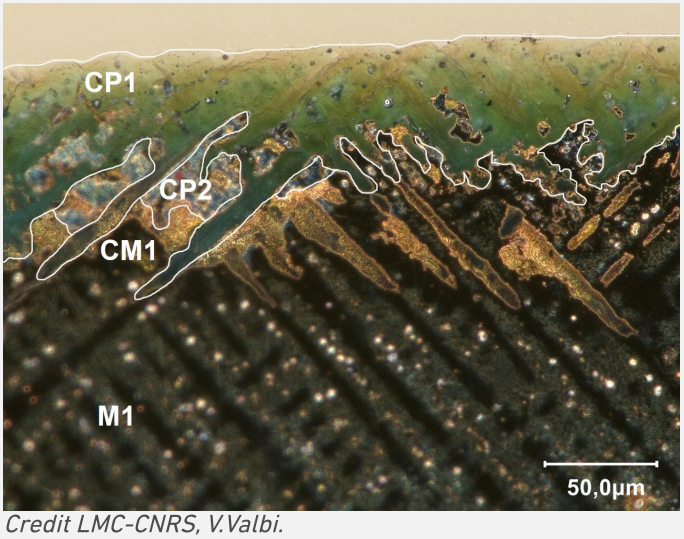
| | CP1 |
|---|---|
| Cu | 15 |
| Sn | 45 |
| O | 29 |
| Pb | 1.6 |
| Si | 3.4 |
| Ca | 2.1 |
| P | 1.9 |
| Fe | 1.1 |
| Cr | <0.5 |
| Ni | <0.5 |
| Cl | < 0.5 |

Table 4: Chemical composition of the corrosion layer over a general area of analysis in cross-section obtained by SEM-EDX.

Analyses with µ-Raman were performed on the identified strata (Fig. 11). The R01 point of analysis was performed on the discontinuous CP2 layer and the obtained spectrum presented the typical main peaks (145, 218, 632 $cm^{-1}$) of the Raman RUFF reference spectrum of cuprite $Cu_2O$ (Lafuente et al. 2015). The R02 point of analysis was performed on

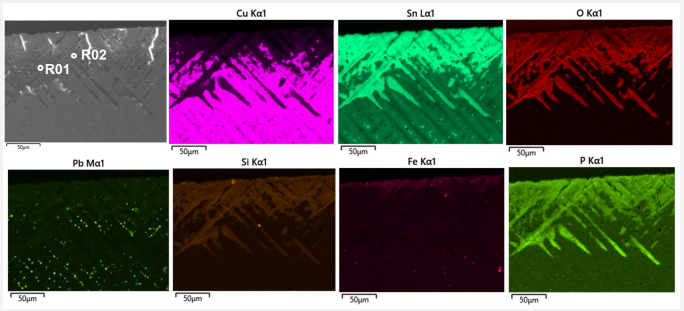

This work is licensed under CC BY-NC-ND 4.0

the green layer and the spectrum obtained has a broad peak at 560 $cm^{-1}$) that can be attributed to nanocrystals of cassiterite $Sn_2O$ thanks to comparison with the work of Ospitali et al. 2012.



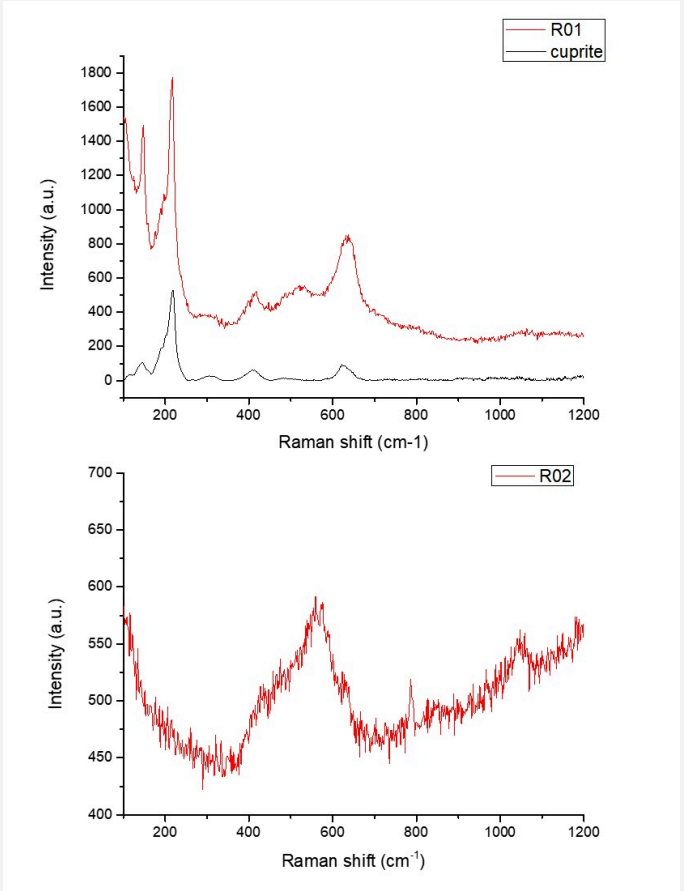

*Credit LMC-CNRS, V.Valbi.*

Fig. 9: Micrograph of the corrosion structure from Fig. 5 (detail): green external CP1, red/gold CP2 following the dendritic structure,




*Credit LMC-CNRS, V.Valbi.*

Fig. 10: SEM image, BSE-mode, and elemental chemical distribution of Fig. 9. The selected points for Raman analysis shown in Fig. 11 are indicated,




*Credit LMC-CNRS, V.Valbi.*

Fig. 11: Raman spectra of points R01 (together with the RRUFF reference RRUFFID=R140763 for cuprite) and R02 showed in Fig. 10,


This work is licensed under CC BY-NC-ND 4.0

| | |
|---|---|
| **Corrosion form** | Multiform - selective |
| **Corrosion type** | Type I (Robbiola) |

**Complementary information**

None.

## MiCorr stratigraphy(ies) – CS

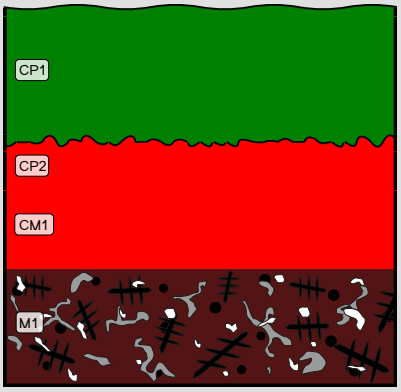


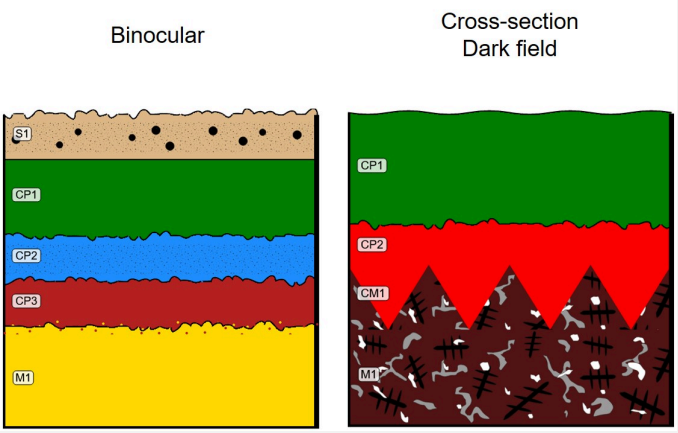

Fig. 12: Stratigraphic representation of the sample of the bracelet observed in cross-section under dark field using the MiCorr application. The characteristics of the strata are only accessible by clicking on the drawing that redirects you to the search tool by stratigraphy representation. This representation was build according to Fig. 9, Credit LMC-CNRS, V.Valbi.

## Synthesis of the binocular / cross-section examination of the corrosion structure

One S and three CPs were identified by binocular observation, while two CPs and a CM were observed in cross-section. It is reasonable to say that the CP1 and CP2 observed in binocular observation correspond to the CP1 observed in cross-section. In fact, in cross-section it is also possible to observe a different shade of green (yellowish) on the outer part of the CP1 that can justify the documentation of two different strata by the conservator. However the difference in color does not correspond in this case to a significant chemical difference, so it was identified as only one stratum in CS. The CP3 layer identified by binocular observation corresponds to the CP2 identified as cuprite in cross-section.

The outer sediment layer (S1), easily identified under binocular, was not visible in the cross-section. On the contrary, the presence of a CM1 stratum was only revealed through cross-section observation. Moreover, information obtained under binocular examination such as brightness, compactness, cohesion, and adherence are not accessible during cross-sectional observation. Conversely, the physico-chemical characteristics obtained by cross-section examination are not easily accessible during the binocular examination. The differences observed underline the necessity and complementarity of these two approaches.


This work is licensed under CC BY-NC-ND 4.0




*Credit HE-Arc CR, N.Gutknecht / LMC-CNRS, V.Valbi.*

Fig. 13: Stratigraphic representation side by side of binocular view and cross-section (dark field),

## Conclusion

The bracelet is a tin bronze with Pb inclusions. The metallographic observation revealed that the metal was cast without additional work, in agreement with the first assessment of this object as a draft of a bracelet. It shows a dendritic microstructure with the presence of eutectic Sn-rich phase.

The characterization of the corrosion products showed a typical corrosion structure for an archeological bronze. The object presents the phenomenon of decuprification with Sn enrichment. This is a common phenomenon observed on bronze archaeological objects buried in moderately aggressive natural conditions (such as oxygenated sandy soils) and accompanied by the formation of cuprite at the interface with the metal. Cuprite is the first compound often to be formed during the corrosion of bronzes (Robbiola et al. 1998, Scott 2006). The enrichment in Ca, Si, P in the CP1 was also previously observed on archaeological objects (Robbiola et al. 1998, Papadopoulou et al. 2016) and can be attributed to the diffusion of these elements from the burial soil.

The good conservation condition of the original surface located, according to the Bertholon's method, at the interface of CP1 with S1 allows to identify the corrosion form as a Type I according to Robbiola et al. 1998 classification. CP1 presents hammering traces and decoration which are typical markers of the original surface.

This bracelet is part of a corpus of four bracelets (bracelet bus-na 98 BZ 11 / bus-na 98 BZ 23 / bus-na 98 BZ 38 / bus-na 98 BZ 67) found in the same site. These artefacts are all drafts of bracelets but correspond to different stages of advancement: two bracelets are "as cast" and present no further working (bracelet bus-na 98 BZ 23 and bus-na 98 BZ 38) while two bracelets present signs of annealing and cold-working (bracelet bus-na 98 BZ 11 and bus-na 98 BZ 67).

## References

**References on object and sample**

1. MiCorr_Bracelet bus-na 98 BZ 11
2. MiCorr_Bracelet bus-na 98 BZ 38
3. MiCorr_Bracelet bus-na 98 BZ 67

**References on analytical methods and interpretation**

4. Bertholon, R. (2001) Characterization and location of the original surface of corroded archaeological objects. Surface Engineering, 17 (3), 241-245.
5. Degrigny, C., Gaspoz, C., Rosselet, A., Boissonnas, V., Jeanneret, R. and Bertholon, R. (2016) The MIFAC-Metal Online project: developing a Decision Support System for locally invasive diagnosis of heritage metals, in METAL 2016, proceedings of the ICOM-CC Metal WG interim meeting, eds. R. Menon, C. Chemello and A. Pandya, New Dehli, (India), 220-227.
6. Lafuente, B., Downs, R. T., Yang, H., Stone, N. (2015) The power of databases: the RRUFF project. In: Highlights in Mineralogical Crystallography, T. Armbruster and R. M. Danisi, eds. Berlin, Germany, W. De Gruyter, 1-30.
7. Ospitali, F., Chiavari, C., Martini, C., Bernardi, E., Passarini, F., Robbiola, L. (2012) The characterization of Sn-based corrosion products in ancient bronzes: a Raman approach. Journal of Raman Spectrpscopy, 43 (11), 1596-1603.
8. Papadopoulou, O., Vassiliou, P., Grassini, S., Angelini, E. and Gouda, V. (2016) Soil-induced corrosion of ancient


This work is licensed under CC BY-NC-ND 4.0

Roman brass – A case study. Materials and Corrosion, 67, No. 2.
9. Scott, D. (2006) Metallography and microstructure of ancient and historic metals. J Paul Getty Museum Publications.
10. Robbiola L., Blengino M., Fiaud C., (1998) Morphology and mechanisms of formation of natural patinas on archaeological Cu–Sn alloys. Corrosion Science, 40 (12), 2083-2111.


This work is licensed under CC BY-NC-ND 4.0